ELSEVIER

Thermochimica Acta 256 (1995) 291–307

thermochimica acta

Combustion of some iron-fuelled binary pyrotechnic systems

Michael J. Tribelhorn, Michael G. Blenkinsop, Michael E. Brown *

Chemistry Department, Rhodes University, Grahamstown 6140, South Africa

Received 18 August 1994; accepted 3 November 1994

Abstract

Combustion studies of several binary pyrotechnic systems using iron powder as fuel and one of the oxidants, BaO_2, SrO_2 or $KMnO_4$, are reported. Temperature profiles were recorded together with simultaneous measurement of burning rates. Burning rates varied with chemical system, with composition and with degree of compaction, and ranged from 2.3 to 39 mm s^{-1} (Fe/BaO_2), 3.3 to 8.3 mm s^{-1} (Fe/SrO_2), and 2.2 to 93 mm s^{-1} (Fe/$KMnO_4$).

Combustion products were examined using scanning electron microscopy, X-ray diffraction (XRD) and infrared spectroscopy.

Approximate kinetic parameters for the combustion reactions of the Fe/peroxide and Fe/permanganate systems were determined using the Leeds approach.

Keywords: Binary system; Iron powder; Pyrotechnic

1. Introduction

The present study complements a detailed thermoanalytical study [1] of the binary Fe/$KMnO_4$, Fe/BaO_2 and Fe/SrO_2 systems, which included the qualitative use of thermomagnetometry as an aid in examining the reactions of iron. The oxidants used in this study (BaO_2, SrO_2 or $KMnO_4$) decompose without melting to produce oxygen gas and a solid residue [1]. Iron powder is oxidised by gaseous oxygen at temperatures (150°C) well below the melting point of iron (1535°C). The

* Corresponding author.

SSDI 0040-6031(94)02190-2

reactions of the pyrotechnic mixtures may thus be either solid–solid or solid–gas reactions.

The use of barium and strontium peroxide in pyrotechnic systems is common and has been briefly reviewed [2]. Spice and Staveley's important study [3,4] included the Fe/BaO_2, $Fe/K_2Cr_2O_7$, S/BaO_2, Mo/BaO_2 and Mn/BaO_2 systems. Potassium permanganate has also been extensively used as an oxidant in pyrotechnic delay compositions [2] and the combustion of several systems has been reported [5,6] to involve two stages of reaction. The first stage (with low activation energy) involves diffusion and interaction along grain boundaries. The second stage involves reaction with the bulk material at higher temperatures. Combustion of the $Sb/KMnO_4$ system [7,8] occurs via gaseous intermediates, including $O_2(g)$ from decomposition of the oxidant, and possibly $Sb_2O_3(g)$.

2. Experimental

2.1. Materials

The materials used were as described in Ref. [1]. The compositions of fuel/oxidant mixtures are given as mass percentages of fuel.

2.2. Apparatus

The equipment used for the measurement of burning rates and temperature profiles has been described [7]. Small-diameter thermocouple wire gives faster response times and decreased heat losses by conduction along the thermocouple wire, but the use of 0.05-mm thermocouples resulted in excessive electrical noise due to movement of the junction during passage of the combustion wave. Correction factors for kinetic data were obtained by extrapolating data measured with thicker thermocouples to zero thermocouple thickness.

Scanning electron microscopy (SEM) (Joel JSM-840) was used to examine the shapes and surface appearance of the individual reactant powders and the reaction residues, and X-ray diffraction (XRD) and infrared spectroscopy were used to try to identify the reaction products.

2.3. Data processing

Temperature profiles were processed in a number of steps. A simple filter program was used to remove deviations caused by noise, and the data were then averaged to reduce the number of points for subsequent processing. Finally, the profiles were smoothed using a 15-point cubic least-squares Savitzky–Golay convolution procedure [9]. Kinetic parameters were derived following the Leeds approach [10,11], which included use of a non-linear optimisation routine in the BMDP statistical software package [12].

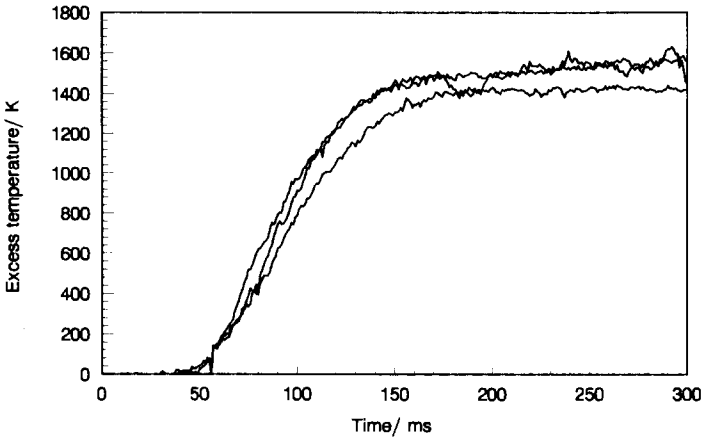

Fig. 1. Replicate temperature profiles for combustion of a 20% Fe/BaO_2 composition, compacted at 55 MPa.

3. Results and discussion

3.1. Combustion of the Fe/BaO_2 system

Compositions containing from 15 to 50% Fe by mass sustained combustion. Fig. 1 illustrates the reproducibility of temperature profiles of one composition (80% Fe/BaO_2) at a compaction pressure of 55 MPa. Profiles have been shifted arbitrarily on the time axis because no fixed zero point exists. The profiles vary in shape (Fig. 2) with composition. Burning rates at 55 MPa ranged from 8.0 to 30 mm s^{-1}, reaching a maximum around 30% (Table 1). The heat outputs per g of mixture,

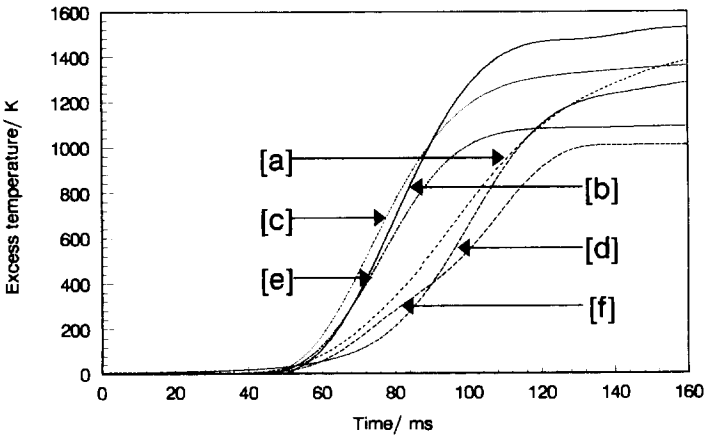

Fig. 2. Temperature profiles for combustion of various compositions of Fe/BaO_2: (a) 15%, (b) 20%, (c) 25%, (d) 30%, (e) 40% and (f) 50% Fe.

Table 1
The effect of composition and compaction pressure on burning rates of the Fe/BaO_2 system

Fe/%	Burning rate/(mm s^{-1}) at different compactions				
	0 MPa	55 MPa	110 MPa	165 MPa	124 MPa [a]
15	2.8 ± 0.9	10.6 ± 1.1	9.1 ± 0.4	9.3 ± 0.1	1.8
20	4.2 ± 1.2	18.1 ± 1.6	16.9 ± 2.4	16.7 ± 2.2	4.6
25	4.7 ± 1.3	20.6 ± 0.9	18.2 ± 0.6	18.0 ± 1.0	6.7
30	5.3 ± 1.1	39.1 ± 8.5	33.6 ± 8.9	26.2 ± 6.2	6.2
35	5.0 ± 0.9	25.5 ± 3.2	18.9 ± 4.1	18.7 ± 2.9	5.3
40	4.3 ± 1.2	14.4 ± 1.2	12.6 ± 2.5	12.5 ± 0.7	4.6
45	3.1 ± 0.8	8.0 ± 0.5	7.8 ± 0.6	7.0 ± 0.5	–
50	2.3 ± 0.9	8.4 ± 0.3	7.0 ± 0.4	3.7 ± 0.3	3.3

[a] Refs. [3,4].

calculated from the measured maximum temperature rises U_{max}, and the heat capacities of the mixtures, reach a maximum around 20% Fe.

Although the burning rates increased with compaction pressure up to 55 MPa, an increase beyond 110 MPa decreased the burning rates (Table 1). Increasing the compaction pressure increases interparticle contact and, hence, the rates of solid–solid reactions, provided that the composition of the mixture is at or near the stoichiometric composition. When solid–gas reactions are involved, increased compaction may decrease the surface of fuel accessible to gas, or compaction may aid in trapping gas which would otherwise move away from fuel surfaces, so simple conclusions cannot be drawn. Fuel/oxidant contact in a solid–solid reaction [13] will be affected far more by composition and particle-size ratios than by compaction (beyond an initial minimum value required).

The method used for preparing pellets in the Spice and Staveley study [3,4] involved the compaction of the mixture at 124 MPa. The 110 MPa series of burning rates obtained in this study should thus show closest correlation to their burning rates, but their values (Table 1) are well below those recorded in this study. The Fe powder (<43 μm, 20 μm range) and the barium peroxide (<20 μm) used in this study were of a considerably finer particle-size than the materials used by Spice and Staveley [3,4] (both fuel and oxidant <150 μm). The effect of compaction on systems with particles larger than the optimum particle size [14] is to increase the interparticle contact while still allowing sufficient interstitial volume for gas flow ahead of the burning front. Drennan and Brown [15] showed that variation of the particle size of the peroxide within the range 10–36 μm had negligible effects on temperature profiles for Mn and Mo/peroxide systems. The different thermal environments, different particle sizes and different chemical purities of the materials used in the two studies could thus explain the lack of agreement of measured burning rates.

Several substances were added separately in small amounts (1–10% by mass) to the binary 20% Fe/BaO_2 composition. These additives were: BaO, $Ba(OH)_2$ and $BaCO_3$ (which are likely contaminants of BaO_2); Fe_2O_3 (formed by some oxidation

of Fe); water (always present on exposure of compositions to the surrounding atmosphere); and Al_2O_3 (a supposedly inert substance, expected only to affect combustion by its action as a diluent). $BaCO_3$ had the least effect on combustion of any of the additives used. Even mixtures which contained in excess of 15% $BaCO_3$ were found to support combustion. $BaCO_3$ formation on the surfaces of BaO_2 may, however, have a greater effect on combustion than the presence of separate $BaCO_3$ particles in the mixture. In contrast to the carbonate, the hydroxide had a large effect on the temperature profiles. Mixtures containing in excess of 5% of the hydroxide did not support combustion. This effect is related to the sensitivity of the system to the presence of water. Dispersion of water throughout the sample presented difficulties, and a standing time of not less than 12 h was allowed for complete dispersion. The addition of water in excess of 1% to the 20% Fe/BaO_2 mixture resulted in no combustion being initiated. BaO_2 particles may become coated with a layer of $Ba(OH)_2$, which inhibits combustion more than having separate particles of $Ba(OH)_2$ interdispersed throughout the mixture. During combustion the water will be regenerated by (endothermic) decomposition of the hydroxide and will affect combustion as a gaseous species, disrupting interparticle contact and transferring heat from reaction sites. Water may also react with the surfaces of the iron particles to produce coatings of oxides and hydroxides.

The simplest reactions likely to be involved in combustion of the Fe/BaO_2 system are

$$2Fe(s) + 3BaO_2(s) \rightarrow Fe_2O_3(s) + 3BaO(s) \quad (1)$$

$$3Fe(s) + 4BaO_2(s) \rightarrow Fe_3O_4(s) + 4BaO(s) \quad (2)$$

$$Fe(s) + BaO_2(s) \rightarrow FeO(s) + BaO(s) \quad (3)$$

For 85% pure BaO_2, the stoichiometric compositions (% by mass of Fe) calculated for the above reactions were: (1) 15.8%, (2) 17.4% and (3) 21.9%. The predicted heat of reaction for reaction (1), using 100% pure reactants and calculated from tabulated enthalpies of formation [16], is -652.7 kJ (or -326.4 kJ per mol Fe, or -217.6 kJ per mol BaO_2, or -1.285 kJ per g BaO_2). Because the stoichiometric composition is 18.03% Fe, 1 g of mixture contains 0.8199 g BaO_2 (85% pure), so the heat output $q = 0.90$ kJ per g mixture.

The following ferrate formation reactions may also occur to some extent, but no enthalpies of formation for the products were found

$$Fe_2O_3(s) + BaO(s) \rightarrow BaFe_2O_4(s) \quad (4)$$

$$FeO(s) + BaO_2(s) \rightarrow BaFeO_3(s) \quad (5)$$

$$Fe(s) + 2BaO_2(s) \rightarrow Ba_2FeO_4(s) \quad (6)$$

$$FeO(s) + 2BaO(s) + BaO_2(s) \rightarrow Ba_3FeO_5(s) \quad (7)$$

The values of $\Delta_{react}H$ calculated from standard enthalpies of formation for reaction (1), leading to simple oxide products, and the predicted adiabatic temperature rises calculated using temperature-dependent values of heat capacities [16], are compared with the corresponding experimental quantities in Table 2.

Table 2
A comparison of the enthalpies of reaction for the Fe/BaO_2 system (per g of mixture), determined from temperature profiles, with values calculated from standard tables

Fe/%	$-\Delta_{react}H$/(kJ g^{-1})			U_{ad}/K	
	Calc. [a]	Expt.	Refs. [3,4]	Calc [b]	Expt.
15	0.877	0.761	1.134	1652	1458
20	0.874	0.858	1.046	1525	1522
25	0.819	0.800	–	1386	1378
30	0.765	0.743	0.891	1269	1257
35	0.710	0.711	–	1149	1184
40	0.655	0.691	0.757	1033	1115
45	0.601	0.685	–	922	1078
50	0.546	0.693	0.686	811	1055

[a] From standard enthalpies of formation [16]. [b] From standard enthalpies of reaction and tabulated heat capacities [16].

The enthalpies of formation of the $BaMnO_4$ and $BaMoO_4$ spinel compounds are slightly more negative than the corresponding formation of simple oxides, indicating that formation of mixed oxides may result in more negative enthalpies of formation than those calculated in Table 3 for the formation of simple Fe oxides and BaO.

Table 3
Kinetic parameters obtained for combustion of the Fe-fuelled pyrotechnic systems

Fe/%	E_a/(kJ mol^{-1})	A/s^{-1}	n
Fe/BaO_2			
15	13.0 ± 1.5	101 ± 15	0.50 ± 0.06
20	13.8 ± 1.8	165 ± 20	0.72 ± 0.09
25	10.2 ± 0.5	120 ± 3	0.51 ± 0.04
30	13.9 ± 1.7	221 ± 67	0.55 ± 0.07
35	15.5 ± 2.6	218 ± 42	0.58 ± 0.07
40	10.7 ± 2.0	271 ± 72	0.64 ± 0.08
45	7.1 ± 0.8	68 ± 12	0.58 ± 0.10
50	10.2 ± 2.1	110 ± 19	0.71 ± 0.19
Fe/SrO_2			
20	20.1 ± 2.3	196 ± 30	0.67 ± 0.04
25	27.0 ± 2.4	191 ± 50	0.73 ± 0.12
30	36.7 ± 8.3	190 ± 9	0.67 ± 0.04
35	41.5 ± 9.2	169 ± 37	0.58 ± 0.11
40	43.5 ± 4.4	349 ± 32	0.63 ± 0.06
45	32.8 ± 3.1	349 ± 35	0.56 ± 0.07
50	31.7 ± 7.1	233 ± 21	0.71 ± 0.05
55	27.9 ± 6.7	257 ± 62	0.75 ± 0.18
50% $Fe/KMnO_4$			
	8.11		0.510

Table 4
Comparison of burning rates from experiment with values predicted from thermal conduction theory for the Fe/BaO_2 system

Fe/%	λ/ (W m^{-1} K^{-1})	c/ (J g^{-1} K^{-1})	ρ/ (g m^{-3})	D/ (m^2 s^{-1})	t_r/ ms	v_{exp}/ (mm s^{-1})	v_{calc}/ (mm s^{-1})	D_{eff}/ (m^2 s^{-1})
15	0.221	0.531	4.10×10^6	1.0×10^{-7}	2.2	10.6	6.7	2.5×10^{-7}
20	0.216	0.573	4.01×10^6	9.4×10^{-8}	1.6	18.1	7.7	5.2×10^{-7}
25	0.153	0.591	3.67×10^6	7.1×10^{-8}	1.2	20.6	7.7	5.1×10^{-7}
30	0.123	0.603	3.50×10^6	5.8×10^{-8}	0.9	39.1	8.0	1.4×10^{-6}
35	0.150	0.618	3.80×10^6	6.4×10^{-8}	1.1	25.5	7.6	7.2×10^{-7}
40	0.155	0.634	3.92×10^6	6.2×10^{-8}	1.6	14.4	6.2	5.3×10^{-7}
45	0.146	0.652	3.88×10^6	5.8×10^{-8}	1.9	8.0	5.5	1.2×10^{-7}
50	0.121	0.673	3.46×10^6	5.2×10^{-8}	2.5	8.4	4.6	1.8×10^{-7}

The maximum heat output predicted from standard enthalpies of reaction is 895 J g^{-1} and occurs at the stoichiometric point of 18% Fe/BaO_2. At higher percentages of fuel, the experimental enthalpy of reaction exceeds the predicted values, possibly because additional reactions giving mixed oxide products occur concurrently.

3.1.1. Kinetics from temperature profiles

Temperature profiles for Fe/BaO_2 compositions were converted into their component power functions [10,11]. For all the Fe/BaO_2 compositions used, only one major peak was observed for the reaction power function G. The activation energies and Arrhenius pre-exponential factors and apparent orders of reaction for the compositions are given in Table 3.

The apparent activation energies are all low values characteristic of diffusion-controlled processes, with lowest values at the highest percentages of fuel. The apparent orders of reaction n are characteristic of contracting-geometry models of solid state reactions [17].

The linear burning rate v of a composition is related to the rise time t_r of the corresponding temperature profile by the expression [11], based on thermal conduction theory, $v = (\lambda/c\rho t_r)^{1/2}$, where λ is the thermal conductivity, c the heat capacity and ρ the density. Each of these quantities depends upon the composition and, to various extents, on the temperature. Values of c and ρ for the mixtures at 298 K may be calculated from tabulated values for the components [16]. Sometimes sufficient information is available to predict values of c at the combustion temperature. Values of λ are more difficult to estimate, especially at high temperatures, and in this study values were estimated using the Kunii–Smith [18] model which has been shown [7] to produce fair agreement with the limited experimental data available.

In Table 4, values of λ, c and ρ for the range of Fe/BaO_2 compositions have been estimated. These may be combined to give thermal diffusivities, $D = \lambda/(\rho c)$. The experimental rise-times t_{rexp} are then combined with the D values to give the

calculated burning rates v_{calc}, which are compared with experimental burning rates v_{exp}.

Agreement between values of v_{calc} and of v_{exp} is, at best, only fair at the extremes of the composition range. The differences between experimental and calculated values of the burning rates may be explained if the effective thermal diffusivities, under combustion conditions (see Table 4), are greater than those predicted, through increased thermal conductivities and/or decreased heat capacities at higher temperatures.

3.2. Combustion of the Fe/SrO_2 system

Compositions containing from 20 to 55% Fe by mass sustained combustion under compaction. This range is similar to that found for Fe/BaO_2 (15–50%). Fig. 3 shows the reproducibility of temperature profiles of the 25% Fe/SrO_2 composition. Comparison of these profiles with those for Fe/BaO_2 (Fig. 1) shows that U_{max} values are about 200°C lower for the Fe/SrO_2 composition, that the overall temperature rises take place over a longer time scale, and that the initial rise region of the profile may involve at least two stages.

Variation in the composition changes the shape of the temperature profiles (Fig. 4) and the maximum temperatures reached by the reaction. Burning rates at 55 MPa ranged from 3.6 to 8.3 mm s^{-1} (Table 5), compared to 8.0 to 39 mm s^{-1} for Fe/BaO_2.

Compaction had relatively little effect on the burning rate (Table 5), compared with that observed for Fe/BaO_2. A tendency of the SrO_2 particles to coalesce on compaction was noted, which could result in uneven dispersal of the peroxide amongst the Fe particles.

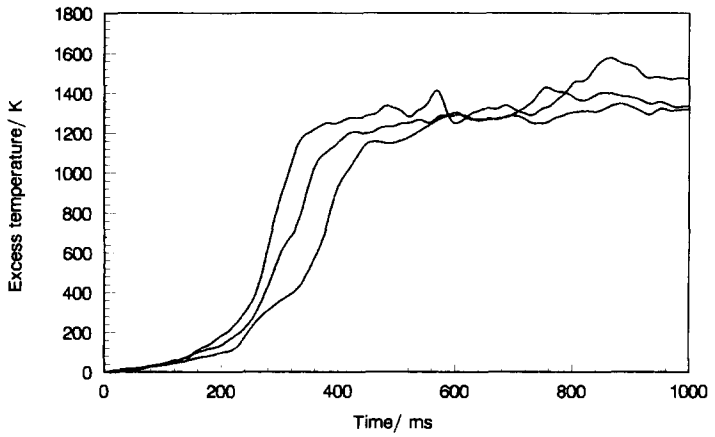

Fig. 3. Replicate temperature profiles for combustion of a 25% Fe/SrO_2 composition, compacted at 55 MPa.

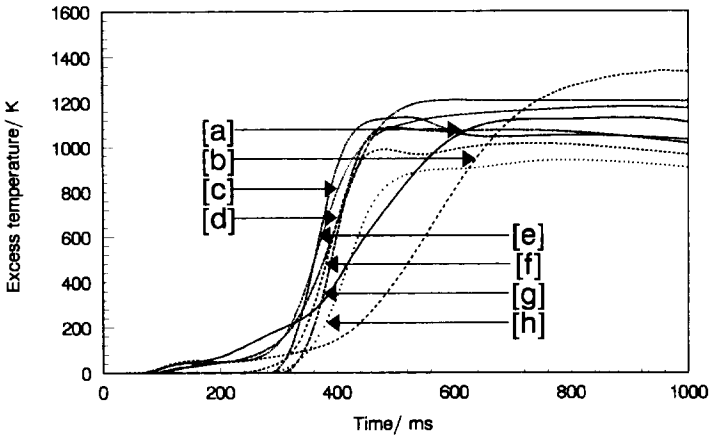

Fig. 4. Temperature profiles for combustion of various compositions of Fe/SrO_2: (a) 20%, (b) 25%, (c) 30%, (d) 25%, (e) 40%, (f) 45%, (g) 50% and (h) 55% Fe.

An analogous set of additives to that used in the study of the Fe/BaO_2 system was tested on the 25% Fe/SrO_2 composition. The substances were: SrO, $Sr(OH)_2$, $SrCO_3$, Fe_2O_3, Al_2O_3 and water. Unlike the BaO_2 system, where $BaCO_3$ had the smallest effect on the burning characteristics of the material, $SrCO_3$ had a major effect. When added in quantities exceeding 1% by mass, mixtures containing $SrCO_3$ failed to support combustion. Formation of $SrCO_3$ on the surfaces of SrO_2 particles may have an even greater effect on combustion than the presence of separate $SrCO_3$ particles dispersed in the mixture. As found for the Fe/BaO_2 system, mixtures containing 1% or more of the hydroxide did not support combustion. Combustion could not be initiated in any of the water-containing systems (the minimum addition was 1% H_2O by mass). This sensitivity of combustion to the presence of water is similar to that found for the Fe/BaO_2 system.

The simplest reactions likely to be involved in combustion of the Fe/SrO_2 system are the strontium analogues of reactions (1)–(3) above. The stoichiometric compositions (% by mass of Fe) calculated for those reactions, for 85% pure SrO_2, are:

Table 5
The effects of composition and compaction on the burning rates (mm s^{-1}) of the Fe/SrO_2 system

Fe/%	0 MPa	55 MPa	110 MPa	165 MPa
20	3.3 ± 1.0	3.6 ± 1.1	3.5 ± 0.9	–
25	6.7 ± 1.8	6.8 ± 1.2	7.0 ± 1.3	5.7 ± 1.1
30	6.8 ± 1.7	7.4 ± 2.0	7.4 ± 1.8	6.2 ± 1.3
35	6.8 ± 1.9	7.5 ± 1.8	7.4 ± 1.7	6.7 ± 1.5
40	7.0 ± 2.1	8.3 ± 1.2	7.8 ± 1.5	6.8 ± 1.4
45	6.5 ± 1.1	6.5 ± 0.6	6.0 ± 0.7	5.4 ± 1.1
50	5.8 ± 1.2	6.3 ± 0.8	5.5 ± 1.1	4.8 ± 0.9
55	5.4 ± 1.2	6.0 ± 0.9	5.2 ± 1.0	4.5 ± 1.2

Table 6
A comparison of the enthalpies of reaction for the Fe/SrO_2 system (per g of mixture), determined from temperature profiles, with values calculated from standard tables

Fe/%	ΔH/(kJ g^{-1})		U_{ad}/K	
	Calc. [a]	Expt.	Calc. [b]	Expt.
20	1.197	1.067	1515	1350
25	1.188	1.041	1483	1300
30	1.109	1.011	1371	1250
35	1.030	0.924	1283	1150
40	0.951	0.887	1180	1100
45	0.871	0.793	1098	1000
50	0.792	0.751	1002	950
55	0.713	0.707	908	880

[a] From tables of standard enthalpies of formation [16]. [b] From standard enthalpies of reaction and tabulated heat capacities [16].

(1) 20.9%, (2) 22.9% and (3) 28.4%. The predicted heat of reaction for 100% pure reactants, calculated from tabulated enthalpies of formation [16] for reaction (1), is −668.9 kJ (or −334.5 kJ per mol Fe or −223.0 kJ per mol SrO, or −1.864 kJ per g SrO_2). Because the stoichiometric mixture is 23.72% Fe, the heat output of the mixture q is 1.21 kJ per g mixture. Again, further reaction at the high temperatures involved (>1000°C) to form ferrite products is possible, but the enthalpies of formation of such products were not available.

The values of $\Delta_{react}H$ calculated from standard enthalpies of formation, for reaction (1) leading to simple oxide products, and the predicted adiabatic temperature rises, calculated using temperature-dependent values of heat capacities [16], are compared with the corresponding experimental quantities in Table 6.

In the Fe/SrO_2 system, the stoichiometric composition for reaction (1) occurs at about 23%, which corresponds with the maximum heat output. The close agreement between the calculated and experimental values of the enthalpy of reaction support the suggestion that the chief products of the reaction are $Fe_2O_3 + 3SrO$.

3.2.1. Kinetics from temperature profiles

Temperature profiles for Fe/SrO_2 compositions were converted into their component power functions [10,11]. For the more reproducible profiles of the Fe/SrO_2 system, only one major peak was observed for the reaction power function G. The activation energies, Arrhenius pre-exponential factors and apparent orders of reaction n for the compositions studied are given in Table 3.

The apparent activation energies are all low values characteristic of diffusion-controlled processes and there is little variation with composition, but values are somewhat larger than those determined for the corresponding Fe/BaO_2 compositions (Table 3). This result is discussed further below. The apparent orders of reaction n lie in a similar range (0.56–0.75) to those found for the Fe/BaO_2 compositions.

As described for the Fe/BaO_2 system, burning rates for the range of Fe/SrO_2 compositions were estimated from the thermal diffusivities, $D = \lambda/(\rho c)$, and the experimental rise times t_{rexp}. The calculated burning-rates v_{calc} are compared with experimental burning rates v_{exp} in Table 7.

Agreement between values of v_{calc} and v_{exp} is poor. The fact that the experimental values recorded exceed the calculated burning rates for all compositions, could be explained if the thermal diffusivities have been underestimated. The effective values of D have been calculated and are listed in Table 7.

3.3. The combustion of the $Fe/KMnO_4$ system

Compositions containing from 20% to 70% Fe by mass sustained combustion under compaction. This range extends to higher fuel contents than found for the Fe/peroxide systems (Tables 1 and 5). The temperature profiles for the $Fe/KMnO_4$ system were noisy. Many of the profiles clearly showed the characteristic step reported by Hill [6]. The step showed up best in the profiles of the compositions having low burning rates. The steps were not consistently relateable to specific time or temperature values. Fig. 5 shows the temperature profiles recorded for a range of $Fe/KMnO_4$ compositions. Values of the maximum temperature rise U_{max} decrease as the proportion of Fe increases. The overall temperature rises take place over a similar time scale to those of the Fe/peroxide systems (Figs. 1 and 3).

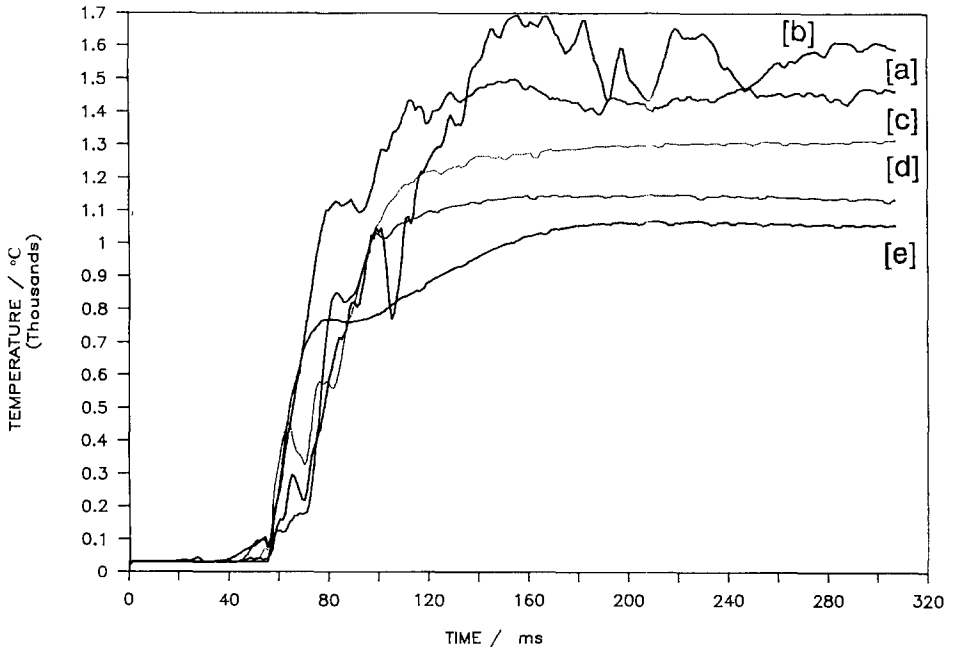

Fig. 5. Temperature profiles for combustion of various compositions of $Fe/KMnO_4$: (a) 30%, (b) 40%, (c) 50%, (d) 60% and (e) 70%.

Table 7
Comparison of burning rates from experiment with values predicted from thermal conduction theory for the Fe/SrO_2 system

Fe/%	λ/(W m^{-1} K^{-1})	c/(J g^{-1} K^{-1})	ρ/(g m^{-3})	D/(m^2 s^{-1})	t_r/ms	v_{exp}/(mm s^{-1})	v_{calc}/(mm s^{-1})	D_{eff}/(m^2 s^{-1})
20	0.130	0.790	3.19×10^6	5.2×10^{-8}	6.3	3.6	2.9	8.2×10^{-8}
25	0.132	0.801	3.28×10^6	5.0×10^{-8}	4.6	6.8	3.3	2.1×10^{-7}
30	0.115	0.809	3.22×10^6	4.4×10^{-8}	3.0	7.4	3.8	1.6×10^{-7}
35	0.109	0.803	3.17×10^6	4.3×10^{-8}	2.5	7.5	4.1	1.4×10^{-7}
40	0.121	0.806	3.36×10^6	4.5×10^{-8}	2.3	8.3	4.4	1.6×10^{-7}
45	0.115	0.793	3.37×10^6	4.3×10^{-8}	2.8	6.5	3.9	1.2×10^{-7}
50	0.126	0.790	3.56×10^6	4.5×10^{-8}	3.8	6.3	3.4	1.5×10^{-7}
55	0.150	0.785	3.86×10^6	5.0×10^{-8}	5.3	6.0	3.1	1.9×10^{-7}

Table 8
The effect of composition on the burning rate (mm s^{-1}) of the $Fe/KMnO_4$ system, and of compaction on the 50% $Fe/KMnO_4$ composition

Fe/%	55 MPa	110 MPa	165 MPa
20	2.20 ± 0.05		
30	6.1 ± 0.8		
40	37.1 ± 35.6		
50	63.6 ± 17.8	75.5 ± 1.5	92.5 ± 3.5
60	17.7 ± 1.6		
70	8.4 ± 0.6		

Burning rates at 55 MPa ranged from 2.2 to 64 mm s^{-1} (Table 8), compared with 8.0 to 39 mm s^{-1} for Fe/BaO_2 and 3.6 to 8.3 mm s^{-1} for Fe/SrO_2.

Spice and Staveley [3,4] found a maximum burning rate of 10.6 mm s^{-1} for the mixture containing 55% Fe. Hill [6] reported a maximum burning rate of 5.5 mm s^{-1}, also at 55% Fe. The present study thus gave considerably higher burning rates. In agreement with Hill [6], the maximum combustion temperature (around 1700°C) was observed for the 40% Fe mixture, suggesting that stoichiometric quantities of reactants are present (assuming the reaction goes to completion). Spice and Staveley [3,4] found maximum generation of heat by the 35% Fe mixture. Enthalpies of reaction for different compositions of the $Fe/KMnO_4$ system are calculated in Table 9.

Burning rates of a 50% Fe mixture increased with loading pressure (Table 8).

Few of the temperature profiles recorded proved to be suitable for kinetic analysis by the Leeds approach. The kinetic parameters obtained from the analysis of a temperature profile for 50% $Fe/KMnO_4$ are given in Table 3. Hill [6] reported a value of 20.7 kJ mol^{-1} for an 80% Fe mixture. Such fuel-rich compositions did not sustain combustion in the present study.

Scanning electron micrographs of the residues of combustion of the 50% Fe composition indicated that little or no melting had occurred.

The TG curves of a loose powdered sample of 50% $Fe/KMnO_4$ heated in air showed a mass loss on decomposition of $KMnO_4$, followed by a mass gain on

Table 9
Enthalpies of reaction for different compositions of the $Fe/KMnO_4$ system. (The heat capacity is based on that of Fe = 0.450 J K^{-1} g^{-1}, and $KMnO_4$ = 0.754 J K^{-1} g^{-1})

Fe/%	$U_{max} = (T - T_a)$/ K	Heat capacity/ (J K^{-1} g^{-1})	Heat of reaction Q/ (kJ g^{-1})
30	1460	0.663	0.97
40	1695	0.632	1.07
50	1288	0.602	0.77
60	1110	0.572	0.63
70	1065	0.541	0.58

oxidation of Fe. The overall mass gain by the mixture was approximately 10%. This suggests operation of a solid–gas–solid mechanism when the mixture burns as a loose powder. This agrees with the mechanism proposed by Hill [6] and Rees [19]. When compacted, the mass of the sample did not change significantly on combustion.

4. Reaction mechanisms

Once fuel/oxidant contact is present, one or more of several possibilities has to occur: (1) atoms or ions derived from A have to move across the A/B interface into the B lattice; (2) atoms or ions derived from B have to move across the B/A interface into the A lattice; (3) species derived from both A and B diffuse simultaneously in opposite directions. Once exothermic reaction has been initiated, the temperature will rise rapidly, at least in the neighbourhood of the sites of initiation. Such temperature rises can produce phase changes and/or oxidant decompositions which can significantly alter the mechanisms and overall course of reaction.

When the fuel is a metal, the oxidant is an oxide or peroxide, and the reaction product is a complex metal oxide, even if usually amorphous in structure, it is most probable that atoms of the metal fuel will diffuse into the oxide or peroxide lattice (with the appropriate electron transfer processes taking place as required). This should occur most readily in excess metal-type oxides. Hill [6] has proposed that this type of mechanism accounts for the two-stage temperature profiles observed for the combustion of several metal/$KMnO_4$ systems. The two stages are proposed to arise from diffusion of metal fuel through (a) structurally defective oxidant, and (b) the bulk of the oxidant of more regular structure. For the finely ground powders used in pyrotechnic systems, a fairly high proportion of oxidant is likely to be defective in structure, but it is of interest to examine initially the possibilities of diffusion of fuel into the regular structures of the oxidants.

The ideal path would be

Fuel A + oxidant B (regular structure) → solid product C (regular structure)

but this will undoubtedly be accompanied (and probably dominated) by the alternative paths

Fuel A + oxidant B (regular structure) → product C (amorphous)

Fuel A + oxidant B (defective structure) → product C (regular structure)

Fuel A + oxidant B (defective structure) → product C (amorphous)

Several complicating factors can intervene:

(a) The oxidant may undergo solid phase changes, melting or decomposition, for example

Oxidant B (regular structure) → product D (usually defective structure) + gases

(b) The fuel A may melt (or even vaporise at high temperatures).

As an initial simplification, the oxidant B will be assumed to be of regular structure and the structure will be approximately maintained during the initial stages of reaction. Whether the fuel A is then present as solid, liquid, or even vapour, will then only influence the ease with which the concentration of A on the surfaces of solid particles of B is maintained.

The BaO_2 and SrO_2 structures have the same space group ($F4/mmm$), with slightly different lattice parameters (BaO_2: $a = b = 0.5384$ nm, $c = 0.6841$ nm; SrO_2: $a = b = 0.5044$ nm, $c = 0.6550$ nm). The stoichiometry of the peroxide decompositions [20] indicates the formation of the oxides, BaO and SrO, and O_2 gas. The structures of BaO and SrO are the same ($Fm\bar{3}m$), again with slightly different lattice parameters (BaO: $a = 0.5520$ nm, SrO: $a = 0.5144$ nm). Loss of oxygen results in a contraction of the unit cells of both oxidants in the c dimension, accompanied by slight expansions in the a and b dimensions. Partial loss of oxygen could create considerable space within the oxidant structure for accommodation of atomic or ionic species derived from the fuel. From the ionic radii, the fcc unit cell parameters of BaO and SrO indicate virtual ionic "contact" along cell edges: BaO has a possible packing size of $2r_{Ba^{2+}} + 2r_{O^{2-}} = 0.532$ nm, with a cell edge of 0.552 nm, while SrO has $2r_{Sr^{2+}} + 2r_{O^{2-}} = 0.488$ nm, with a cell edge of 0.514 nm. The well-documented formation of complex oxides, using alkaline-earth peroxides as reactants with other simple metal oxides, confirms the ease of movement of cations in a matrix of oxide ions. It is thus possible to speculate on the species which are most likely to diffuse in solid–solid reactions.

X-ray powder diffraction studies of the products of the Fe/BaO_2 and Fe/SrO_2 reactions indicate the formation of some $Ba_3Fe_2O_6$ and $BaFe_2O_4$, and $Sr_3Fe_2O_{6.16}$, respectively (along with unreacted reactants and some BaO and SrO). In the $Ba_3Fe_2O_6$ structure, Fe has an oxidation state of +3. A starting point for consideration then, would be the movement of an Fe^{3+} ion into the BaO_2 structure. The radius of an Fe atom is 0.126 nm, and of an Fe^{3+} ion 0.055 nm. The Ba^{2+} ion has a radius of 0.134 nm, so an Fe atom could be accommodated in a Ba^{2+} vacancy. The radius of an Sr^{2+} ion is 0.112 nm, so accommodation of an Fe atom in an Sr^{2+} vacancy would be more difficult. It is thus likely that either Fe^{3+} is formed by surface oxidation of iron particles and that these ions can then transfer to oxidant particles, or that Fe atoms may be accommodated initially in cation vacancies at the oxide surface, undergo electron transfer and then move into the structure as Fe^{3+}.

The activation energies recorded for the Fe/BaO_2 and Fe/SrO_2 systems (Table 3) are relatively low, in accordance with the values expected for diffusion-based reactions. The values of the BaO_2 system vary between 10 and 16 kJ mol^{-1}, while the values of SrO_2 are slightly higher at 20–42 kJ mol^{-1}. The lower activation energies recorded for the Fe/BaO_2 system could support the suggestion that diffusion of Fe in the BaO_2/BaO lattice occurs more readily than in the SrO_2/SrO lattice. By comparison, the activation energies found [15] for the Mn/BaO_2, Mo/BaO_2 and Mn/SrO_2 systems at 20% by mass of fuel were between 16 and 22 kJ mol^{-1}, and that of Mo/SrO_2, 38 kJ mol^{-1} at 40% fuel.

Although binary pyrotechnic systems are initially solid–solid mixtures, much effort has been directed to determining whether the major contribution to the combustion reaction occurs in the condensed phase as a solid–solid, solid–liquid or liquid–liquid reaction, or whether gaseous intermediates are involved. Pyrotechnic delay systems for use in sealed detonator tubes must be essentially gaseous. The Fe/BaO_2 system was identified almost 40 years ago, by Spice and Staveley [3,4], as such a system. Thermomagnetometry (TM) has been used [1] to provide additional information about the system. The TG curves for the oxidation of Fe show a final mass gain corresponding to the formation of Fe_2O_3 as expected. TM shows the Curie point of Fe_3O_4 around 580°C. A magnetic event at $\approx$340°C probably arises from the surface formation of some ferromagnetic γ-Fe_2O_3, which converts to paramagnetic α-Fe_2O_3 at about this temperature. TG curves for both Fe/oxidant systems, heated in powder form at 20°C min^{-1} in N_2, showed superimposition of the oxidation of Fe on the decompositions of the oxidants. DTA traces showed strongly exothermic processes corresponding to ignition. The TM traces showed the same features as that of Fe in air, suggesting that reaction under these conditions is solid–gas with little or no interaction between Fe and the solid oxidants. In some mixtures the presence of unreacted Fe was apparent from the Curie point of Fe at 780°C. Fe/oxidant pellets behaved differently from loose powders, but there was no conclusive evidence for solid–solid reaction mechanisms. Most of the observations could be explained by trapping of the gaseous products of oxidant decomposition within the pellets.

The physical properties of the SrO_2 particles, including the mean particle size ($\approx$3 μm vs. <20 μm for BaO_2) resulted in a tendency for these particles to coalesce. This may affect the degree of mixing with fuels during preparation of pyrotechnic mixtures, ultimately affecting the degree of completion of reaction. The differences between the behaviour of BaO_2 and SrO_2 with the same fuel must arise mainly from chemical factors. The decompositions $SrO_2(s) \rightarrow SrO(s) + 0.5O_2(g)$ and $BaO_2(s) \rightarrow BaO(s) + 0.5O_2(g)$ [20] are considerably different so that availability of oxygen for a solid–gas reaction would be different in the two combinations.

The Fe/oxidant reactions appear to be more vigorous than $Fe/O_2(g)$. Reasons for this could be: (1) local high-pressure pockets of $O_2(g)$ formed by decomposition of the oxidant and trapped within the powder, and/or (2) some kind of surface process where the partially oxidised surface of the Fe particles may be activated by reaction with neighbouring oxidant particles or a gaseous species (for example H_2O) generated on heating the oxidant. Water in relatively large amounts inhibits reaction, due to the reactivity of both the fuels and the peroxides with H_2O.

Any potential use which the Fe/peroxide systems may have as delay compositions, with burning rates of from 3 to 30 mm s^{-1}, is offset by the susceptibility of the oxidants to reaction with water and CO_2 in the atmosphere. Combustion of the Fe/peroxide systems was very susceptible to the presence of added or absorbed water.

An additional aim of this study was to determine whether combustion processes could lead to the formation of useful solid residues. For example, combustion of the iron/peroxide systems could be considered as a self-propagating high-temperature

synthesis (SHS) route [21] to the production of ferrites with their useful electronic applications. All the techniques used (SEM, XRD, EPMA) showed, however, the heterogeneity of the solid residues of combustion. Hence, even if SHS was suitable as a first stage in the production of ferrite materials (or other complex oxides), there would still have to be a more conventional treatment involving grinding of the residue, possible adjustment of compositions, and calcining.

Acknowledgements

The authors are indebted to Dr R.A. Rugunanan for his interest and comments, and to AECI Explosives Ltd. for financial support.

References

[1] M.E. Brown, M.J. Tribelhorn and M.G. Blenkinsop, J. Therm. Anal., 40 (1993) 1123.
[2] M.J. Tribelhorn, D.S. Venables and M.E. Brown, Thermochim. Acta, 256 (1995) 309.
[3] J.E. Spice and L.A.K. Staveley, J. Soc. Chem. Ind., 68 (1949) 313.
[4] J.E. Spice and L.A.K. Staveley, J. Soc. Chem. Ind., 68 (1949) 348.
[5] R.A.W. Hill and A.A. Wallace, Nature, 178 (1956) 692.
[6] R.A.W. Hill, Trans. Faraday Soc., 53 (1957) 1136.
[7] M.W. Beck and M.E. Brown, 10th Int. Pyrotech. Sem., Fraunhofer Inst. für Treib- und Explosivstoffe, 1985, paper 14.
[8] M.W. Beck and M.E. Brown, Comb. Flame, 65 (1986) 67, 263.
[9] A. Savitzky and M.J.E. Golay, Anal. Chem., 36 (1964) 1627.
[10] T. Boddington, P.G. Laye, J.R.G. Pude and J. Tipping, Comb. Flame, 47 (1982) 235.
[11] T. Boddington, P.G. Laye, J. Tipping and D. Whalley, Comb. Flame, 63 (1986) 359.
[12] W.J. Dixon, BMDP statistical software manual, University of California Press, 1988.
[13] M.E. Brown and S.J. Taylor, in preparation.
[14] J. Subrahmanyam and M. Vijakumar, J. Mater. Sci., 27 (1992) 6249.
[15] R.L. Drennan and M.E. Brown, Thermochim. Acta, 208 (1992) 201, 223, 247.
[16] R.C. Weast, Handbook of Chemistry and Physics, CRC Press, Florida, 67th edn., 1986.
[17] M.E. Brown, D. Dollimore and A.K. Galwey, Comprehensive Chemical Kinetics, Vol. 22, Elsevier, Amsterdam, 1980.
[18] D. Kunii and J.M. Smith, J. Am. Inst. Chem. Eng., 6 (1969) 71.
[19] G. Rees, Fuel, 52 (1973) 138.
[20] M.J. Tribelhorn and M.E. Brown, Thermochim. Acta, submitted, TCA 2156.
[21] Z.A. Munir and J.B. Holt (Eds.), Combustion and Plasma Synthesis of High-Temperature Materials, VCH Publishers, New York, 1990.